STRENGTHS AND PLASTIC SHRINKAGE CRACKING RESISTANCE OF MORTAR OVERLAYS INCORPORATING STEEL SLAG AND RUBBER AGGREGATES FOR CONCRETE PAVEMENT REPAIR

Phat Nguyen, Phuong N. Pham*

The University of Danang – University of Science and Technology, Vietnam

*Corresponding author: pnphuong@dut.udn.vn

(Received: April 29, 2025; Revised: June 05, 2025; Accepted: June 18, 2025)

DOI: 10.31130/ud-jst.2025.23(9B).517E

Abstract - This paper investigated the compressive strength, flexural tensile strength, abrasion resistance, and resistance to plastic shrinkage cracking of mortar overlay for concrete pavements with three sand replacement ratios by volume: control (no incorporation), 30% steel slag (30SSA), 30% rubber aggregates (30RA), and a combination of 15% SSA and 15% RA (15SSA15RA). The results indicate that most mixtures satisfied the flexural strength requirement (> 4 MPa) and exhibited adequate abrasion resistance for all road classifications (< 0.3 g/cm²), except for the mortar incorporating 30% RA, which failed to achieve the required flexural capacity. Notably, the mortar with SSA revealed a higher resistance to plastic shrinkage cracking. The 15SSA15RA mixture, in particular, exhibited no visible cracks, demonstrating its effectiveness in mitigating shrinkage and resulting cracking when incorporating SSA and RA. The findings promotes the application of rubber-steel slag mortar in concrete pavement repair for the sustainable reuse of by-products in road construction.

Keywords - Mortar overlay; concrete pavement repair; steel slag aggregates; rubber aggregates; plastic shrinkage cracking

1. Introduction

Concrete pavement is widely used for roads with high traffic volumes and heavy loads, as well as in areas with frequent braking and adverse hydrothermal conditions. However, various types of pavement deterioration occur after use, including corner cracking, transverse cracking, joint damage, surface wear, slipperiness, spalling, and aggregate exposure [1]. To address these issues, TCCS 12:2016/ TCĐBVN recommends the application of either a thin bituminous mortar or an ultra-thin asphalt concrete overlay to enhance surface texture [2]. However, due to fundamental differences in the mechanical behavior between asphalt-based and cement-based materials, further deterioration may occur, such as delamination caused by poor adhesion between cement and asphalt concrete and reflective cracking at joints from the existing concrete pavement [3].

Numerous studies have proposed using thin cement-based or geopolymer overlays to address these issues [4]. These overlays enhance pavement quality and extend service life compared to asphalt concrete [5]. The bond strength between the overlay and the existing cement concrete pavement plays a crucial role in the durability of the interface and in preventing premature failure [6]. Overlay materials, the existing pavement surface conditions, and the surface treatment method significantly influence the bond performance [7]. Gholami et al. [8] investigated a cementitious repair material combined with a calcium chloride accelerator, which improved adhesion to cement concrete pavement, achieving bond strengths of 1.4–2.7 MPa. Additionally, several approaches, such as using geopolymer with fly ash [9], polymer combined with glass powder and steel slag [10], and surface treatment through sandblasting [11], have demonstrated significant potential in enhancing adhesion performance.

Various international standards specify a minimum bond strength requirement for practical pavement applications ranging from 1.0 to 1.5 MPa [12] - [14]. Additionally, overlay mixtures should develop strength rapidly, minimize shrinkage, and reduce the likelihood of cracking. However, geopolymer materials exhibit high shrinkage rates, compromising long-term durability [15]. Several studies have demonstrated that steel slag aggregates (SSA) and rubber aggregates (RA) can mitigate shrinkage and reduce resulting cracking [16] - [19]. To date, no research has investigated the combined use of waste-derived aggregates, such as SSA and RA, in mortar overlays, particularly under plastic shrinkage conditions, which represent a critical early-age stage where cracks are likely to develop shortly after placement. Therefore, this study focuses on evaluating the effects of steel slag and rubber aggregates on compressive strength, flexural tensile strength, abrasion resistance, and, particularly, resistance to plastic shrinkage cracking when these by-products were partially replaced for fine aggregates in thin mortar overlays for the repair of cement concrete pavements.

2. Materials and methods

2.1. Materials

The cement mortar overlay mixture includes river sand, cement, water, and admixtures. Electric arc furnace SSA (0.075–4.75 mm) sourced from Da Nang Steel Company was sieved in the laboratory to meet the particle size distribution requirements of ASTM C33/C33M [20]. The SSA had a specific gravity of 3.07 g/cm³ and a water absorption rate of 10.09%. The RA (1–3 mm) was derived from recycled waste tires provided by Long Long Rubber Recycling Vietnam, with a specific gravity of 1.2 g/cm³ and negligible water absorption.

In this study, SSA and RA partially replace river sand (0.075–4.75 mm), which has a fineness modulus of 3.2 and a specific gravity of 2.64 g/cm³ due to the similarity in particle size distribution between river sand and RA as well

as SSA (Figure 1). The PCB 40 cement, having a 3-day compressive strength of 38.3 MPa, a setting time of 140–185 minutes, a specific gravity of 3.1 g/cm³, and a standard water requirement of 31%, was used and met requirements according to TCVN 6262:2020 [21]. Sikament NN was applied to adjust the slump of all mixtures to a range of 5–7.5 cm [5].

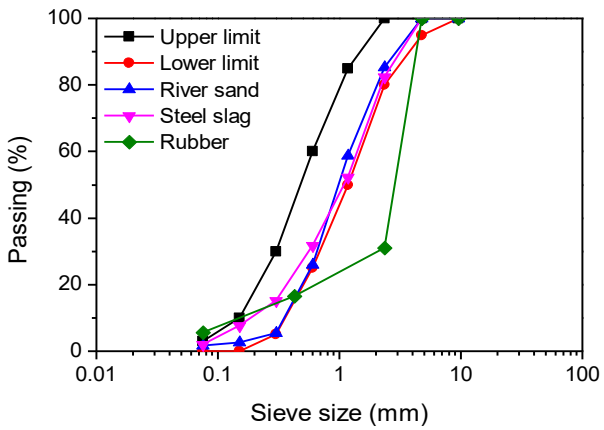

Figure 1. *Gradation curves of different aggregates*

2.2. Mixture design and specimen preparation

The thin mortar overlay was designed based on previous research to ensure adequate bond strength, workability, and durability. According to Zailani et al. [9], the optimal mortar mix with a binder-to-sand ratio of 1:2 achieved the highest bond strength. The mixture was designed to achieve rapid strength development, minimize expansion and shrinkage, and produce fast-setting concrete with a high binder content and a low water-to-cement ratio, thereby optimizing adhesion and workability [5]. The water-to-cement ratio was selected at 0.38 [7]. To enhance the properties of the mortar overlay, this study proposes three mix designs in which river sand is partially replaced by SSA (30SSA), RA (30RA), or a combination of both by-products (15SSA15RA) by volume. The material quantities were determined using Equation (1), where $m_{SSA(RA)}$ $p_{SSA(RA)}$ $\gamma_{SSA(RA)}$ and γ_{sand} are the mass, percentage, and bulk density of SSS (or RA) and sand, respectively. As a result, four mortar mix designs were proposed, as presented in Table 1.

$$m_{SS(RA)} = p_{SS(RA)} \frac{\gamma_{SS(RA)}}{\gamma_{sand}} m_{sand} \quad (1)$$

Table 1. *Mix proportions of mortar overlays (kg/m³)*

Mix	W/C	C	W	Sand	SSA	RA	SP
0SSA0RA	0.38	684.9	260.2	1369.7	-	-	4.1
30SSA	0.38	684.9	260.2	958.8	477.8	-	4.2
30RA	0.38	684.9	260.2	958.8	-	186.8	-
15SSA15RA	0.38	684.9	260.2	958.8	238.9	93.4	-

C: Cement, W: Water, SP: Superplasticizer

This study focuses on compressive strength, flexural tensile strength, abrasion resistance, and resistance to plastic shrinkage cracking. Compressive and flexural tensile strength tests were conducted on specimens measuring 4 cm × 4 cm × 16 cm, while 7 cm × 7 cm × 7 cm cubic specimens were used for abrasion resistance testing. The river sand was washed to remove impurities, and SSA was soaked in water for 24 hours, rinsed, and surface-saturated before mixing. First, sand, SSA, and RA were dry-mixed using a 50-liter mixer. Subsequently, 70% of the total water was added to achieve initial moisture, while the remaining 30% was mixed with the superplasticizer to ensure uniform dispersion and accomplish the target slump. The mix was poured into molds in two layers. Each layer was compacted using a vibrating table until air bubbles were evenly released on the surface. Afterward, it proceeded to the next layer, or the surface was swiped. The specimens were moist-cured for 24 hours before demolding and then water-cured until the designated testing ages.

2.3. Experimental methods

2.3.1. Compressive strength and flexural strength tests

The compressive strength (f_k) and flexural tensile strength (f_t) were conducted according to TCVN 3121:2003 [22], using a mortar compression machine with a maximum load capacity of 100 kN. The samples were subjected to compression at a rate of 3 kN/s until complete failure, while the flexural test was performed at a loading rate of 50 N/s. For samples with a compressive capacity exceeding 100 kN, a 500-kN compression machine was used with a similar loading rate. The failure modes observed after compression or flexion were used to evaluate the failure mechanisms of mortar overlays incorporating SSA or RA.

a) Compression *b) Flexion* *c) Abrasion*

Figure 2. *Fundamental properties of mortar overlay*

2.3.2. Abrasion resistance test

The abrasion resistance test was conducted on naturally dry specimens according to TCVN 3114:2022 [23] using a grinder (Figure 2c). The experimental procedure consists of the following steps:

(i) Weigh the initial mass of the two naturally-dry specimens.

(ii) Place the specimens in the grinder, ensuring that the top surface is evenly in contact with the grinding plate.

(iii) Position the specimen and apply a load pressure of 0.06 MPa.

(iv) Rotate the grinding disc at a speed of 30 rpm and simultaneously sprinkle 20 g of standard sand along the 30-meter grinding path. After every five repetitions, corresponding to one cycle of 150-m grinding, the specimen is rotated by 90° in the same direction.

(v) Clean the sample after four grinding cycles have ended and measure its remaining mass.

The abrasion loss M_m (g/cm²) is calculated using

Equation (2), where m_0 is the initial mass of the specimen (g), m_4 is the remaining mass after four grinding cycles (g). F is the ground surface area of the specimen in contact with the abrasive disc (cm²), measured with a precision of 0.01 cm before testing.

$$M_m = \frac{m_o - m_4}{F} \quad (2)$$

2.3.3. Plastic shrinkage cracking resistance test

The test aims to evaluate resistance to plastic shrinkage cracking according to GB/T 50082:2009 standard [24], using a bone mold with dimensions and shape as illustrated in Figure 3a. The specimens were prepared by first pouring the mix into the mold a half and vibrating until air bubbles were evenly released on the surface. A similar process was applied to the second layer. The surface of the specimen was then smoothed and subjected to a continuous air stream for 24 hours at a wind speed of at least 5 m/s (Figure 3b). All specimens were tested at room temperature under uniform conditions to eliminate the influence on shrinkage behavior. After this period, the formation of cracks was observed, and their positions were identified, marked, and measured. Parameters such as crack length, width, and depth were measured using a ruler and recorded to assess the effect of SSA and RA on the resistance of the resulting mortar overlay to crack resistance.

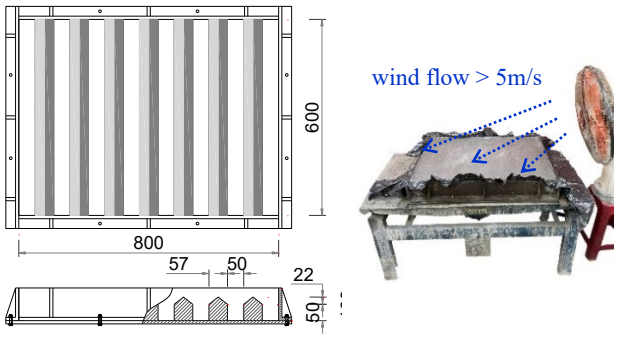

Figure 3. *Mold for plastic shrinkage test (a) and induction of continuous airflow on surface (b)*

3. Results and discussion

3.1. Compressive strength and flexural tensile strength

Figure 4 and Figure 5 show a decrease in compressive strength and flexural tensile strength of the mortar overlay when river sand is replaced with SSA and RA. The control mix achieved a 28-day compressive strength of 69.17 MPa, while the 30SSA, 30RA, and 15SSA15RA mixes reached 53.42 MPa, 23.33 MPa, and 31.86 MPa, respectively. For flexural tensile strength, although the mixes showed a decrease at 1 day and 7 days when part of the sand was replaced with the by-products, the 30SSA mix still maintained a value comparable to the control sample at 28 days, consistent with the findings of Kim et al. [25]. Except for the 30RA mix, all other mixes meet the flexural strength requirements for concrete pavements subjected to loads exceeding 100 kN, as specified in TCCS 40:2022/TCĐBVN [26].

Figure 6 shows the failure modes of mortar specimens after flexion damage. The 30SSA mix exhibited a brittle fracture mechanism similar to that of the control mix, whereas the rubberized mixes showed more ductile behavior, especially 30RA. The reduction in the strength of the mortar overlay using RA can be attributed to the decreased density, low hardness, and poor adhesion between RA and the cement matrix [27], [28]. SSA has a porous structure, a rough surface, and high porosity, which increases water absorption [29]. Hence, SSA can be beneficial or detrimental to the properties of cement-based composites [30]. Notably, SSA may negatively impact the compressive strength of high-strength concrete, whereas in normal-strength concrete, SSA can improve compressive strength [18], [30].

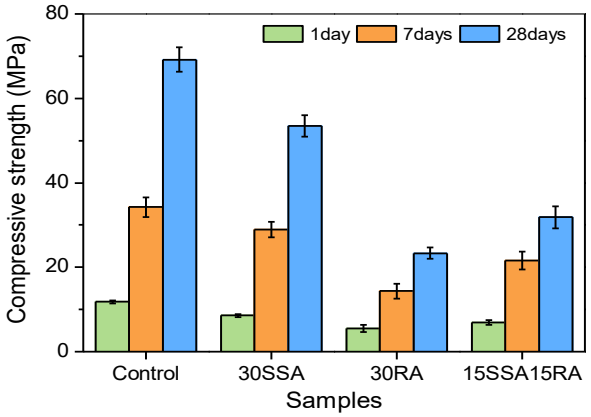

Figure 4. *Effect of SSA and RA on compressive strength of overlay mortar*

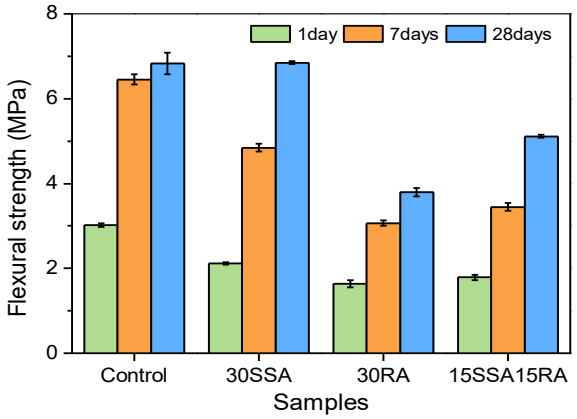

Figure 5. *Effect of SSA and RA on flexural tensile strength of overlay mortar*

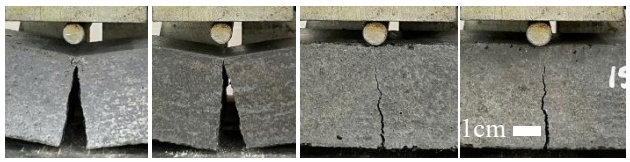

a) Control *b) 30SSA* *c) 30RA* *d) 15SSA15RA*

Figure 6. *The failure mode of specimens under flexural tension*

3.2. Abrasion loss

Figure 7 presents the abrasion loss for the various mortar overlays, where the control mix shows the least abrasion value of 0.181 (g/cm²), while the 30SSA, 30RA, and 15SSA15RA achieve 0.267 (g/cm²), 0.213 (g/cm²), and 0.204 (g/cm²), respectively. The increased abrasion when using RA can be explained by the poor bond between

RA and the cement matrix [28]. In contrast, the porous structure with discontinuous crystals [29], many organic impurities, a high proportion of flat, elongated particles, and a high Los Angeles can explain the reduction in resistance of SSA mortar to abrasion [18], [19]. These characteristics are detrimental to the durability of mortar overlay, especially under severe abrasion conditions. Still, all mixes meet the abrasion limit for concrete pavements (< 0.3 g/cm²) according to TCCS 40:2022/TCĐBVN [26].

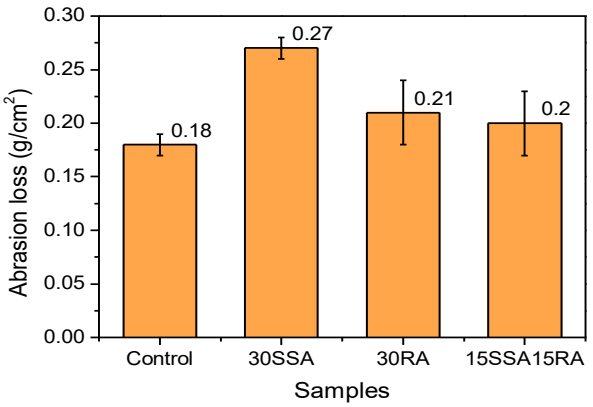

Figure 7. *Effect of SSA and RA on the abrasion resistance of cementitious overlay at 28 days*

3.3. Cracking resistance due to plastic shrinkage

Figure 8 shows that shrinkage cracking became evident after the designed mortar was exposed to windy conditions for 24 hours. The control mix exhibited a severe cracking level, with the length of the full-depth crack and surface crack reaching 1384 mm and 4391 mm, respectively, indicating a high sensitivity of the mix to shrinkage cracking. In contrast, the use of SSA to replace river sand in 30SSA significantly reduced plastic shrinkage crack development, as evidenced by the reduced lengths of the through-crack and surface crack to 395 mm and 2256 mm, respectively, corresponding to reductions of 28.5% and 51.4% compared to the control mix. This phenomenon can be explained by the high water absorption of SSA, which helps maintain internal moisture content, thereby supporting the internal curing process of the slag-delivered mortar. Moreover, the width of the through-crack in 30SSA and the control mix showed no significant difference (0.9 mm), which is consistent with the flexural test results (Figure 5) and observed failure modes (Figure 6). The details of cracking resistance due to plastic shrinkage are summarized in Table 2. However, toughness value, energy absorption, and crack formation mechanisms remain unaddressed and warrant further investigation.

Notably, 15SSA15RA showed no cracking under adverse conditions during the 24-hour curing period. This result demonstrates the superior effectiveness of incorporating SSA and RA into the shrinkage cracking resistance of the mortar overlay. RA acts as a natural expansion joint system, significantly enhancing the resistance of rubberized cement-based composites to shrinkage. The combination of SSA and RA in the cement mortar provides an optimal solution for reducing plastic shrinkage cracking, contributing to the sustainability of the overlay under actual exposure conditions.

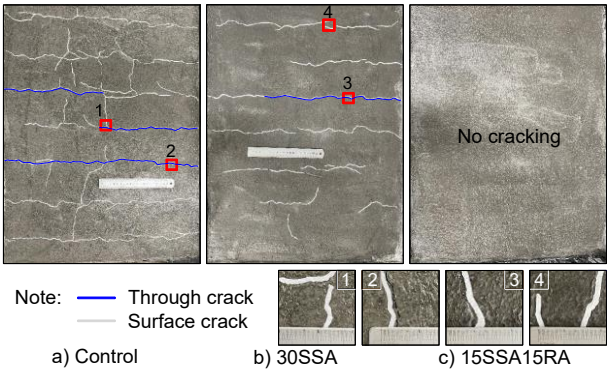

Figure 8. *Plastic shrinkage cracking in cement mortar overlay mixtures*

Table 2. *Parameters of plastic shrinkage cracking in pavement mortar overlay*

Mix specimen	Control	30SSA	15SSA15RA
Through-crack length (mm)	1384	395	0
Surface crack length (mm)	4391	2256	0
Maximum crack depth (mm)	28	28	0
Maximum crack width (mm)	0.9	0.9	0

4. Conclusion

This paper investigates the fundamental properties of cement mortar overlays used for concrete pavement surface repair, where SSA and RA are used to replace river sand by volume. Through assessment of compressive strength, abrasion resistance, and shrinkage cracking resistance, the following main conclusions are drawn:

- Replacing river sand with SSA and RA reduces the compressive strength of the mortar overlay. Still, such reduction does not affect the performance of concrete pavement overlay repair, except for 30RA, as the main requirements of the overlay are flexural strength and abrasion resistance.

- The flexural strength of the mortar overlay using SSA is comparable to that of the control sample, while RA reduces this property. However, the 15SSA15RA mix still meets the strength requirements for overlays under traffic conditions with an axle load not exceeding 100 kN.

- RA has little impact on abrasion resistance, while SSA shows a more pronounced effect. Nonetheless, the proposed mixes still meet the limit for concrete pavements (< 0.3 g/cm²).

- The shrinkage cracking resistance of the mortar overlay is significantly improved when SSA and RA are used. Notably, the 15SSA15RA exhibited no plastic shrinkage cracks.

Reusing SSA and RA enhances specific properties of mortar overlay, reduces environmental impact, promotes a circular economy, and supports green and sustainable construction. Further research focuses on dry shrinkage and its resulting impact on cracking resistance, bond strength, and the microstructural interaction between the mortar overlay and the deteriorated concrete pavement. In addition, the long-term durability and aging behavior of the mortar overlays under operation conditions will be investigated in future studies.

Acknowledgments: Phat Nguyen was funded by the Master Scholarship Programme of Vingroup Innovation Foundation (VINIF), code VINIF.2023.ThS.103.

REFERENCES

[1] F. Liu, B. Pan, C. Zhou, and J. Nie, "Repair interface crack resistance mechanism: A case of magnesium phosphate cement overlay repair cement concrete pavement surface", *Dev. Built Environ.*, vol. 17, p. 100355, 2024, doi: 10.1016/j.dibe.2024.100355.

[2] *Repair of jointed plain concerte pavement - specifications for construction and acceptance*, TCCS 12:2016/TCĐBVN, pp. 1–51, 2016.

[3] Z. Zhao, X. Guan, F. Xiao, Z. Xie, P. Xia, and Q. Zhou, "Applications of asphalt concrete overlay on Portland cement concrete pavement", *Constr. Build. Mater.*, vol. 264, p. 120045, 2020, doi: 10.1016/j.conbuildmat.2020.120045.

[4] A. Manawadu, P. Qiao, and H. Wen, "Characterization of Substrate-to-Overlay Interface Bond in Concrete Repairs: A Review", *Constr. Build. Mater.*, vol. 373, no. March, 2023, doi: 10.1016/j.conbuildmat.2023.130828.

[5] National Concrete Pavement Technology Center, "Guide to Concrete Overlay Solutions", *www.concreteparking.org*, 2007, [Online]. Available: https://www.concreteparking.org/downloads/guide_concrete_overlays.pdf [Accessed April 02, 2025].

[6] S. Austin, P. Robins, and Y. Pan, "Shear bond testing of concrete repairs", *Cem. Concr. Res.*, vol. 29, no. 7, pp. 1067–1076, 1999, doi: 10.1016/S0008-8846(99)00088-5.

[7] M. Rith, Y. K. Kim, S. W. Lee, J. Y. Park, and S. H. Han, "Analysis of in situ bond strength of bonded concrete overlay", *Constr. Build. Mater.*, vol. 111, pp. 111–118, 2016, doi: 10.1016/j.conbuildmat.2016.02.062.

[8] S. Gholami, J. Hu, and Y. R. Kim, "Assessment of bonding, durability, and low-temperature performance of cement-based rapid patching materials for pavement repair", *Int. J. Pavement Eng.*, vol. 24, no. 2, pp. 1–11, 2023, doi: 10.1080/10298436.2022.2120990.

[9] W. W. A. Zailani, N. M. Apandi, A. Adesina, U. J. Alengaram, M. A. Faris, and M. F. M. Tahir, "Physico-mechanical properties of geopolymer mortars for repair applications: Impact of binder to sand ratio", *Constr. Build. Mater.*, vol. 412, p. 134721, 2024, doi: 10.1016/j.conbuildmat.2023.134721.

[10] K. Momeni, N. I. Vatin, M. Hematibahar, and T. H. Gebre, "Repair overlays of modified polymer mortar containing glass powder and composite fibers-reinforced slag: mechanical properties, energy absorption, and adhesion to substrate concrete", *Front. Built Environ.*, vol. 10, pp. 1–10, 2024, doi: 10.3389/fbuil.2024.1479849.

[11] M. A. Al-Osta, S. Ahmad, M. K. Al-Madani, H. R. Khalid, M. Al-Huri, and A. Al-Fakih, "Performance of bond strength between ultra-high-performance concrete and concrete substrates (concrete screed and self-compacted concrete): An experimental study", *J. Build. Eng.*, vol. 51, p. 104291, 2022, doi: 10.1016/j.jobe.2022.104291.

[12] *Products and systems for the protection and repair of concrete structures – Part 3: Structural and non-structural repair*, EN 1504-3, Eur. Comm. Stand. (CEN), Brussels, Belgium, 2005.

[13] C. Sprinkel, M. M. ; Ozyildirim, "Evaluation of hydraulic cement concrete overlays placed on three pavements in Virginia", *Proc. Int. Conf. Concr. Pavements*, vol. 3, no. August, p. 662, 2000, doi: doi.org/10.33593/iccp.v7i1.254.

[14] B. Bissonnette, L. Courard, H. Beushausen, D. Fowler, M. Trevino, and A. Vaysburd, "Recommendations for the repair, the lining or the strengthening of concrete slabs or pavements with bonded cement-based material overlays", *Mater. Struct. Constr.*, vol. 46, no. 3, pp. 481–494, 2013, doi: 10.1617/s11527-012-9929-8.

[15] F. Li, Q. Chen, Y. Lu, Y. Zou, and S. Li, "Mitigating drying shrinkage and enhancing mechanical strength of fly ash-based geopolymer paste with functionalized MWCNTs grafted with silane coupling agent", *Cem. Concr. Compos.*, vol. 143, no. March, p. 105250, 2023, doi: 10.1016/j.cemconcomp.2023.105250.

[16] P. N. Pham, Y. Zhuge, A. Turatsinze, A. Toumi, and R. Siddique, "Application of rubberized cement-based composites in pavements: Suitability and considerations", *Constr. Build. Mater.*, vol. 223, pp. 1182–1195, 2019, doi: 10.1016/j.conbuildmat.2019.08.007.

[17] N. P. Pham, A. Toumi, and A. Turatsinze, "Rubber aggregate-cement matrix bond enhancement: Microstructural analysis, effect on transfer properties and on mechanical behaviours of the composite", *Cem. Concr. Compos.*, vol. 94, pp. 1–12, 2018, doi: 10.1016/j.cemconcomp.2018.08.005.

[18] C. T. Nguyen, P. N. Pham, H. P. Nam, and P. Nguyen, "Factors affecting compressive strength of steel slag concrete : A systematic literature review", *J. Build. Eng.*, vol. 100, p. 111686, 2025, doi: 10.1016/j.jobe.2024.111686.

[19] P. Pham, C. T. Nguyen, and P. Hao, "Mechanical properties, plastic shrinkage cracking resistance and water absorption of paving concrete using steel slag and rubber aggregates", *Journal of Science and Technology in Civil Engineering (JSTCE) - HUCE,* vol. 17, 2023, doi: 10.31814/stce.huce2023-17(2V)-12.

[20] *Standard specification for concrete aggregates*, ASTM C33-C33M, 2018.

[21] *Blended porland cements*, TCVN 6260:2020, 2020.

[22] *Mortar for masonry - Test methods*, TCVN 3121:2003, pp. 1–33, 2003.

[23] *Hardened concrete - Test method for abrasion*, TCVN 3114:2022, 2022.

[24] *Standard for test methods of long-term performance and durability of ordinary concrete*, GB/T 50082:2009, pp. 3–46, 2009.

[25] S. W. Kim, Y. J. Lee, Y. J. Jung, J. Y. Lee, and K. H. Kim, "Applicability of electric arc furnace oxidizing slag aggregates for RC columns subjected to combined bending and axial loads", *Mater. Res. Innov.*, vol. 18, pp. S2793–S2798, 2014, doi: 10.1179/1432891714Z.000000000560.

[26] *Specitications for construction and acceptance of portland cement concrete pavement for highway*, TCCS 40:2022/TCĐBVN, pp. 1–62, 2022.

[27] T. M. Pham *et al.*, "Dynamic compressive properties of lightweight rubberized geopolymer concrete", *Constr. Build. Mater.*, vol. 265, p. 120753, 2020, doi: 10.1016/j.conbuildmat.2020.120753.

[28] S. Zhai *et al.*, "Investigation on the influence of modified waste rubber powder on the abrasion resistance of concrete", *Constr. Build. Mater.*, vol. 357, p. 129409, 2022, doi: 10.1016/j.conbuildmat.2022.129409.

[29] I. Santamaría-Vicario, A. Rodríguez, S. Gutiérrez-González, and V. Calderón, "Design of masonry mortars fabricated concurrently with different steel slag aggregates", *Constr. Build. Mater.*, vol. 95, pp. 197–206, 2015, doi: 10.1016/j.conbuildmat.2015.07.164.

[30] Y. Guo, J. Xie, J. Zhao, and K. Zuo, "Utilization of unprocessed steel slag as fine aggregate in normal- and high-strength concrete", *Constr. Build. Mater.*, vol. 204, pp. 41–49, 2019, doi: 10.1016/j.conbuildmat.2019.01.178.